

Study of isospin violating ϕ excitation in $e^+e^- \rightarrow \omega\pi^0$

Gang Li^{1,3}, Yuan-Jiang Zhang^{1,3} and Qiang Zhao^{1,2,4}

1) *Institute of High Energy Physics, Chinese Academy of Sciences, Beijing 100049, P.R. China*

2) *Department of Physics, University of Surrey, Guildford, GU2 7XH, United Kingdom*

3) *Graduate University of Chinese Academy of Sciences, Beijing 100049, P.R. China and*

4) *Theoretical Physics Center for Science Facilities,
Chinese Academy of Sciences, Beijing 100049, P.R. China*

(Dated: January 21, 2021)

We study the reaction $e^+e^- \rightarrow \omega\pi^0$ in the vicinity of ϕ mass region. The isospin-violating ϕ excitation is accounted for by two major mechanisms. One is electromagnetic (EM) transition and the other is strong isospin violations. For the latter, we consider contributions from the intermediate hadronic meson loops and ϕ - ρ^0 mixing as the major mechanisms via the t and s -channel transitions, respectively. By fitting the recent KLOE data, we succeed in constraining the model parameters and extracting the $\phi \rightarrow \omega\pi^0$ branching ratio. It shows that the branching ratio is sensitive to the ϕ excitation line shape and background contributions. Some crucial insights into the correlation between isospin violation and Okubo-Zweig-Iizuka (OZI) rule evading transitions are also learned.

PACS numbers: 12.40.Vv, 13.20.Gd, 13.25.-k

I. INTRODUCTION

The e^+e^- annihilation at low energies, below 3 GeV, is a major source of information on the properties of light vector mesons (ρ, ω, ϕ) and their excited states. Recently, the cross sections of $e^+e^- \rightarrow \omega\pi^0$ are measured by KLOE collaboration in the vicinity of ϕ -resonance [1, 2], where a dip appears at the ϕ mass. It greatly improves the experimental status for the isospin-violating ϕ meson production in the e^+e^- annihilation. Meanwhile, the significant difference in the extraction of the $\phi \rightarrow \omega\pi^0$ branching ratio in Refs. [1, 2] suggests how difficult to measure such a tiny effect in e^+e^- annihilations. This transition is correlated with the Okubo-Zweig-Iizuka (OZI) rule violation due to the nearly-ideal flavor mixing between ω and ϕ . Since the reaction $e^+e^- \rightarrow \omega\pi^0$ is dominated by the $I = 1$ transition matrix element, the interferences due to the ϕ production will provide an opportunity for probing the isospin-violating mechanism and its correlation with the OZI rule.

In Ref. [3], the isospin-violating decay $\phi \rightarrow \omega\pi^0$ has been studied in an effective Lagrangian approach. Two mechanisms are quantified as the major sources for isospin violations. One is the electromagnetic (EM) transition where the $s\bar{s}$ annihilates into a virtual photon and then decays into ω and π^0 . At leading order, the transition can be accounted for by virtual photon exchange between isoscalar and isovector mesons in vector meson dominance (VMD) model. The isospin conserved vertices can be well constrained by experimental data for $\omega \rightarrow \gamma\pi^0$, $\omega \rightarrow e^+e^-\pi^0$, $\phi \rightarrow e^+e^-\pi^0$, and $\phi \rightarrow \rho\pi + 3\pi$ [4]. The other is the strong isospin violation originated from the u - d quark mass difference due to chiral symmetry breaking of QCD vacuum [5]. A dynamic process to recognize this is via the OZI-rule-evading intermediate meson loop transitions [3].

In this work we study the ϕ meson excitation in $e^+e^- \rightarrow \omega\pi^0$ in the effective Lagrangian approach in order to further improve our understanding of the strong isospin violation mechanism. In contrast with $\phi \rightarrow \omega\pi^0$ [3], more transition mechanisms will be involved in and contribute to $e^+e^- \rightarrow \omega\pi^0$. Detailed analysis of those background contributions will be carried out. Compared with other approaches via π - η mixing or empirical ϕ - ω - ρ^0 mixing [6, 7, 8, 9, 10, 11], our model is based on explicit experimental facts and constructed in a self-consistent way at the tree level of the effective Lagrangian approach.

As follows, we first analyze the mechanism for $I = 1$ transitions in the VMD model. We then include the interferences from the $I = 0$ ϕ production based on the improved prescription of Ref. [3]. Numerical results are presented in Sec. III and a summary is given in Sec. IV.

II. THE MODEL

A. $I = 1$ transitions in VMD model

The $I = 1$ EM transition amplitudes are described by isovector meson fields. In the energy region around M_ϕ mass, the dominant contributions are due to the low-lying vector mesons, such as ρ^0 , $\rho'(1450)$, etc. In the VMD model [12], we can decompose the virtual photon by these mesons, e.g. ρ and ρ' , as shown in Fig. 1(a) and (b). The transition amplitudes corresponding to Fig. 1(a) and (b) are as follows:

$$M_{fi}^a = \bar{v}^{(s')}(p'_e)(-ie\gamma^\beta)u^s(p_e)\frac{-1}{s(s - M_\rho^2 + i\Gamma_\rho(s)\sqrt{s})}\frac{eM_\rho^2}{f_\rho}\frac{g_{\omega\rho\pi}}{M_\omega}\varepsilon_{\alpha\beta\mu\nu}p_\rho^\alpha p_\omega^\mu \varepsilon_\omega^\nu, \quad (1)$$

$$M_{fi}^b = \bar{v}^{(s')}(p'_e)(-ie\gamma^\beta)u^s(p_e)\frac{-1}{s(s - M_{\rho'}^2 + i\Gamma_{\rho'}(s)\sqrt{s})}\frac{eM_{\rho'}^2}{f_{\rho'}}\frac{g_{\omega\rho'\pi}}{M_{\rho'}}\varepsilon_{\alpha\beta\mu\nu}p_{\rho'}^\alpha p_\omega^\mu \varepsilon_\omega^\nu, \quad (2)$$

where eM_V^2/f_V is a direct photon-vector-meson coupling in Feynman diagram language and $g_{\omega\rho\pi}$ and $g_{\omega\rho'\pi}$ are the VVP strong coupling constants. $\Gamma_\rho(s)$ and $\Gamma_{\rho'}(s)$ are energy-dependent total widths for the intermediate ρ and ρ' , respectively. They are described by the two major decay modes, $\pi^+\pi^-$ and $\omega\pi^0$ [13]:

$$\Gamma_\rho(s) = \Gamma_\rho(M_\rho^2)\frac{M_\rho^2}{s}\left(\frac{p_\pi(s)}{p_\pi(M_\rho^2)}\right)^3 + \frac{g_{\omega\rho\pi}^2}{12\pi M_\omega^2}p_\omega^3(s), \quad (3)$$

$$\Gamma_{\rho'}(s) = \Gamma_{\rho'}(M_{\rho'}^2)\left[\mathcal{B}_{\rho'\rightarrow\omega\pi^0}\left(\frac{p_\omega(s)}{p_\omega(M_{\rho'}^2)}\right)^3 + (1 - \mathcal{B}_{\rho'\rightarrow\omega\pi^0})\frac{M_{\rho'}^2}{s}\left(\frac{p_\pi(s)}{p_\pi(M_{\rho'}^2)}\right)^3\right], \quad (4)$$

where the coupling constant $g_{\omega\rho\pi}/M_\omega$ is taken to be 17 GeV^{-1} , which is the fitted value using three different fitting schemes in Ref. [13]. This value is consistent with the experimental values derived from $\omega \rightarrow \pi^0\gamma$, $\rho \rightarrow \pi^0\gamma$ and $\omega \rightarrow \rho\pi \rightarrow \pi^+\pi^-\pi^0$ decays, and theoretical estimates based on the QCD sum rules [14, 15, 16].

It should be noted that the second term of Eq. (3) does not contribute below the $\omega\pi^0$ threshold. For $\rho'(1450)$, its total and partial widths still have large uncertainties [4]. Its best known decay channel is $\omega\pi$. Therefore, we parameterize its energy-dependent total width into two parts, i.e. $\rho' \rightarrow \omega\pi$ and ρ' decay into other final states. $\mathcal{B}_{\rho'\rightarrow\omega\pi^0}$ is the branching ratio of $\rho' \rightarrow \omega\pi^0$. In the consequent calculation, we will fix $\Gamma_\rho(M_\rho^2) = 149.6 \text{ MeV}$ and take $\Gamma_{\rho'}$ as a parameter due to its large uncertainties.

In the above treatment, we assume that the dominant contributions to the $I = 1$ component are from ρ and ρ' in the energy around M_ϕ mass. Contributions from higher $I = 1$ states should be largely suppressed since their mass are larger than the virtuality of the photon. So, the $I = 1$ total transition amplitude can be expressed as:

$$M_{fi}^{I=1} = M_{fi}^a + e^{i\delta_1} M_{fi}^b, \quad (5)$$

where a possible relative phase between these two amplitudes is included and will be determined by experimental data. We mention in advance that the dominant $I = 1$ background requires $\delta_1 = 180^\circ$ as a constructive phase between ρ and ρ' terms in Eq. (5).

B. $I = 0$ transitions

As studied in Ref. [3], the excitation of ϕ meson can couple to $\omega\pi^0$ via two isospin violation processes. One is EM transitions through ϕ meson annihilation. The other is OZI-evading intermediate meson loops. We separately investigate these two processes in this section. We also consider background amplitudes from the off-shell ω meson excitations.

1. $I = 0$ EM transitions in VMD model

The excitations of the ϕ and ω meson contribute to the signal and background, respectively. We decompose the virtual photon by a sum of vector mesons as shown in Fig. 1(c) and (d). The corresponding amplitudes have the following expressions:

$$\begin{aligned} \mathcal{M}_{fi}^{c-V} &= \sum_{V_1, V_2} \bar{v}^{(s')}(p'_e)(-ie\gamma^\nu)u^s(p_e) \frac{1}{s^2(s - M_{V_1}^2 + i\Gamma_{V_1}(s)\sqrt{s})(s - M_{V_2}^2 + i\Gamma_{V_2}(s)\sqrt{s})} \\ &\times \left(\frac{eM_{V_1}^2}{f_{V_1}}\right)^2 \frac{eM_{V_2}^2}{f_{V_2}} \frac{g_{\omega V_2 \pi}}{M_\omega} \varepsilon_{\alpha\beta\mu\nu} p_\omega^\alpha \varepsilon_\omega^\beta p_\pi^\mu, \end{aligned} \quad (6)$$

and

$$\begin{aligned} \mathcal{M}_{fi}^{d-V} &= \sum_{V_1, V_2} \bar{v}^{(s')}(p'_e)(-ie\gamma^\nu)u^s(p_e) \frac{1}{s(s - M_{V_1}^2 + i\Gamma_{V_1}(s)\sqrt{s})(p_\omega^2 - M_{V_2}^2 + i\Gamma_{V_2}(M_\omega^2)M_\omega)M_\omega^2} \\ &\times \frac{eM_{V_1}^2}{f_{V_1}} \frac{eM_{V_2}^2}{f_{V_2}} \frac{eM_\omega^2}{f_\omega} \frac{g_{V_1 V_2 \pi}}{M_\phi} \varepsilon_{\alpha\beta\mu\nu} p_\omega^\alpha \varepsilon_\omega^\beta p_\pi^\mu, \end{aligned} \quad (7)$$

where V_1 denotes ϕ or ω mesons, while V_2 denotes ρ or ρ' mesons; $g_{V_1 V_2 \pi}$ are the VVP strong coupling constants and $\Gamma_V(s)$ is the total width of the intermediate vector mesons. The $V\gamma$ coupling values can be found in Ref. [17]. The width $\Gamma_\phi(s)$ is described by its major decay modes, K^+K^- , $K_L^0 K_S^0$ and $\rho\pi + \pi^+\pi^-\pi^0$:

$$\begin{aligned} \Gamma_\phi(s) &= \Gamma_\phi(M_\phi^2) \left[\mathcal{B}_{\phi \rightarrow K^+K^-} \frac{M_\phi^2}{s} \left(\frac{p_{K^+}(s)}{p_{K^-}(M_\phi^2)} \right)^3 + \mathcal{B}_{\phi \rightarrow K_L^0 K_S^0} \frac{M_\phi^2}{s} \left(\frac{p_{K_L^0}(s)}{p_{K_L^0}(M_\phi^2)} \right)^3 \right. \\ &\quad \left. + (1 - \mathcal{B}_{\phi \rightarrow K^+K^-} - \mathcal{B}_{\phi \rightarrow K_L^0 K_S^0}) \left(\frac{p_\rho(s)}{p_\rho(M_\phi^2)} \right)^3 \right], \end{aligned} \quad (8)$$

where $\mathcal{B}_{\phi \rightarrow K^+K^-}$, $\mathcal{B}_{\phi \rightarrow K_L^0 K_S^0}$ are the branching ratios of $\phi \rightarrow K^+K^-$, $\phi \rightarrow K_L^0 K_S^0$, respectively. Coupling $g_{\phi\rho^0\pi^0} = 0.68$ is extracted [3] from the KLOE result for $\phi \rightarrow \rho\pi + \pi^+\pi^-\pi^0$ [18].

The relative sign between ρ and ρ' intermediate vector mesons is the same as $I = 1$ transitions, and there is a relative sign δ_2 between the processes Fig. 1 (c) and (d), i.e.

$$\mathcal{M}_{fi}^{EM-I=0} = (\mathcal{M}_{fi}^{c-\rho} + e^{i\delta_2} \mathcal{M}_{fi}^{d-\rho}) + e^{i\delta_1} (\mathcal{M}_{fi}^{c-\rho'} + e^{i\delta_2} \mathcal{M}_{fi}^{d-\rho'}). \quad (9)$$

In the calculation we fix $\delta_2 = 0^\circ$ as given by the effective Lagrangians, while $\delta_1 = 180^\circ$ is required as a constructive phase between the transitions mediated by ρ and ρ' in Fig. 1 (c) and (d).

2. $I = 0$ transitions via intermediate meson loops

The strong isospin violation via the OZI-rule-evading intermediate meson loop transitions can be established by two experimental observations. One is the obvious mass difference between the charged and neutral kaon as a consequence of the u - d quark-mass difference. The other is the precise measurement of the $\phi \rightarrow K^+K^-$ and $K_L K_S$ branching ratios, where the effective couplings of ϕK^+K^- and $\phi K^0 \bar{K}^0$ turn to be slightly different. Therefore, we can describe the strong isospin violation as a dynamic outcome of Fig. 2 for which the detailed mechanisms can be recognized by transitions via Fig. 3. In particular, transitions of Fig. 3(a)-(d) can be classified as t -channel processes, while (e) and (f) are s -channel ones.

In both kinds of transitions, the u - d quark-mass difference leads to the mass difference between the charged and neutral kaon, which then results in nonvanishing $I = 1$ cancellations between the charged and neutral kaon loops as a source of the strong isospin violations in $\phi \rightarrow \omega\pi^0$. Contributions from

$K\bar{K}^*(K)$ and $K\bar{K}^*(K^*)$ loops are also considered in the t -channel where the effective couplings for the charged and neutral particles are treated in the SU(3) symmetry limit as a leading approximation. The s -channel transitions of Fig. 3(e) and (f) contribute to the mixing of the ϕ and ρ^0 , which were not considered in Ref. [3]. However, we state in advance that their contributions are not as large as the t -channel transitions. In this work, in order to keep this effective Lagrangian approach self-consistent, we explicitly include the s -channel $K\bar{K}$ loop in the calculation. The contributions from the $K\bar{K}^* + c.c.$ loops in the s channel are found even smaller since their mass threshold is higher than the ϕ mass. Therefore, we do not consider them in the later discussions.

In principle, we should include all the possible intermediate meson exchange loops in the calculation. In reality, the break-down of the local quark-hadron duality allows us to pick up the leading contributions as a reasonable approximation [19, 20]. As explained in Ref. [3], the leading contributions arise from $K\bar{K}(K^*)$, $K\bar{K}^*(K)$ and $K\bar{K}^*(K^*)$ intermediate meson loops (see Fig. 4). We note that in Ref. [21] the $K\bar{K}(K^*)$ loop was also studied as a major mechanism for ϕ - ρ mixing.

As follows, we present the transition amplitudes for these meson loops in $e^+e^- \rightarrow \omega\pi^0$. The detailed expressions for the loop integrals for the t -channel transitions have been given in Ref. [3]. Hence, we only list the necessary formulas here.

The transition amplitude for $e^+e^- \rightarrow \phi \rightarrow \omega\pi^0$ via an intermediate meson loop can be expressed as:

$$M_{fi} = \bar{v}^{(s')}(p'_e)(-ie\gamma^\rho)u^s(p_e) \frac{-ig_{\rho\sigma}}{s} \frac{eM_\phi^2}{f_\phi} \frac{i\varepsilon_\phi^\sigma}{s - M_\phi^2 + i\Gamma_\phi(s)\sqrt{s}} \int \frac{d^4p_2}{(2\pi)^4} \sum_{K^*pol} \frac{T_1 T_2 T_3}{a_1 a_2 a_3} \mathcal{F}(p_2^2). \quad (10)$$

where the vertex functions for $K\bar{K}(K^*)$ are

$$\begin{cases} T_1 \equiv ig_1(p_1 - p_3) \cdot \varepsilon_\phi \\ T_2 \equiv \frac{ig_2}{M_\omega} \varepsilon_{\alpha\beta\mu\nu} p_\omega^\alpha \varepsilon_\omega^\beta p_2^\mu \varepsilon_2^\nu \\ T_3 \equiv ig_3(p_\pi + p_3) \cdot \varepsilon_2 \end{cases} \quad (11)$$

where g_1 , g_2 , and g_3 are the coupling constants at the meson interaction vertices (see Fig. 4). The four vectors, p_ϕ , p_ω , and p_{π^0} are the momenta for the initial ϕ and final state ω and π meson; The four-vector momentum, p_1 , p_2 , and p_3 are for the intermediate mesons, respectively, while $a_1 = p_1^2 - m_1^2$, $a_2 = p_2^2 - m_2^2$, and $a_3 = p_3^2 - m_3^2$ are the denominators of the propagators of intermediate mesons.

The vertex functions for the $K\bar{K}^*(K) + c.c.$ loop in Fig. 4(b) are

$$\begin{cases} T_1 \equiv \frac{if_1}{M_\phi} \varepsilon_{\alpha\beta\mu\nu} p_\phi^\alpha \varepsilon_\phi^\beta p_3^\mu \varepsilon_3^\nu, \\ T_2 \equiv if_2(p_1 - p_2) \cdot \varepsilon_\omega, \\ T_3 \equiv if_3(p_\pi - p_2) \cdot \varepsilon_3. \end{cases} \quad (12)$$

where $f_{1,2,3}$ are the coupling constants.

Similarly, we have vertex functions for the intermediate $K\bar{K}^*(K^*) + c.c.$ loop (Fig. 4(c)):

$$\begin{cases} T_1 \equiv \frac{ih_1}{M_\phi} \varepsilon_{\alpha\beta\mu\nu} p_\phi^\alpha \varepsilon_\phi^\beta p_3^\mu \varepsilon_3^\nu, \\ T_2 \equiv \frac{ih_2}{m_2} \varepsilon_{\alpha'\beta'\mu'\nu'} p_2^{\alpha'} \varepsilon_2^{\beta'} p_\omega^{\mu'} \varepsilon_\omega^{\nu'}, \\ T_3 \equiv \frac{ih_3}{m_3} \varepsilon_{\alpha''\beta''\mu''\nu''} p_2^{\alpha''} \varepsilon_2^{\beta''} p_3^{\mu''} \varepsilon_3^{\nu''} \end{cases} \quad (13)$$

where $h_{1,2,3}$ are the coupling constants.

In the above three kinds of vertex functions, the coupling constants are determined via experimental value and SU(3) relations [3, 4, 22]. The form factor $\mathcal{F}(p^2)$, which takes care of the off-shell effects of the exchanged particles [23, 24, 25], is usually parameterized as

$$\mathcal{F}(p^2) = \left(\frac{\Lambda^2 - m_{ex}^2}{\Lambda^2 - p^2} \right)^n, \quad (14)$$

where $n = 0, 1, 2$ correspond to different treatments of the loop integrals. In the present work, we only consider the monopole form factor, i.e. $n = 1$. For the cut-off energy Λ , it is usually parameterized:

$$\Lambda = m_{ex} + \alpha\Lambda_{QCD}, \quad (15)$$

where $\Lambda_{QCD} = 220$ MeV and α is a tunable parameter, m_{ex} is the mass of exchanged meson. We note that this form of form factor is slightly different from that adopted in Ref. [3]. It smooths out the integrals in terms of a varying Λ value.

3. $I = 0$ transitions via ϕ - ρ^0 and ω - ρ^0 strong mixings

The $I = 0$ transitions via the s -channel ϕ - ρ^0 and ω - ρ^0 strong mixings are shown in Fig. 5. The amplitude for ϕ - ρ^0 mixing via the charged kaon loop can be expressed as follows:

$$\begin{aligned} M_{fi}^c &= \bar{v}(p_{e+})(-ie\gamma_a)u(p_{e-}) \frac{g_{ab}(-g^{bc} + \frac{p_\phi^b p_\phi^c}{M_\phi^2})}{s(s - M_\phi^2 + i\Gamma_\phi(s)\sqrt{s})} \frac{eM_\phi^2}{f_\phi} g_{\phi K^+ K^-} g_{\rho K^+ K^-} \\ &\times \int \frac{d^4 p_2}{(2\pi)^4} \frac{4p_{2c} p_{2d}}{(p_1^2 - m_1^2)(p_2^2 - m_2^2)} \frac{-ig^{df}}{s - M_\rho^2 + i\Gamma(s)\sqrt{s}} \frac{ig_{\omega\rho\pi}}{M_\omega} \epsilon_{efgh} p_\pi^e p_\omega^g \epsilon_\omega^h \\ &= -\bar{v}(p_{e+})(-ie\gamma^f)u(p_{e-}) \frac{1}{s(s - M_\phi^2 + i\Gamma_\phi(s)\sqrt{s})} \frac{eM_\phi^2}{f_\phi} g_{\phi K^+ K^-} g_{\rho K^+ K^-} \\ &\times \frac{|\vec{P}_1|^3}{6\pi\sqrt{s}} \frac{1}{s - M_\rho^2 + i\Gamma(s)\sqrt{s}} \frac{g_{\omega\rho\pi}}{M_\omega} \epsilon_{efgh} p_\pi^e p_\omega^g \epsilon_\omega^h, \end{aligned} \quad (16)$$

where an on-shell approximation following the Cutkosky rule has been taken and \vec{P}_1 is the three-vector momentum of the on-shell kaon in the meson loop.

Taking into account the charge-neutral term, the amplitude can be written as

$$\begin{aligned} M_{fi} &= \bar{v}(p_{e+})(-ie\gamma^f)u(p_{e-}) \frac{1}{s(s - M_\phi^2 + i\Gamma_\phi(s)\sqrt{s})} \frac{eM_\phi^2}{f_\phi} \\ &\times \epsilon_{\phi\rho} \frac{g_{\omega\rho\pi}}{M_\omega} \epsilon_{efgh} p_\pi^e p_\omega^g \epsilon_\omega^h, \end{aligned} \quad (17)$$

where $\epsilon_{\phi\rho}$ is the strong isospin-violating coupling strength between ϕ and ρ^0 ,

$$\epsilon_{\phi\rho} \equiv \frac{1}{6\pi\sqrt{s}D_\rho} \left[g_{\phi K^+ K^-} g_{\rho K^+ K^-} P_{K^+ K^-}^3(s) + g_{\phi K^0 \bar{K}^0} g_{\rho K^0 \bar{K}^0} P_{K^0 \bar{K}^0}^3(s) \right], \quad (18)$$

where $D_\rho \equiv D_\rho(s) = M_\rho^2 - s - i\sqrt{s}\Gamma_\rho(s)$ and $P_{K^+ K^-}$ and $P_{K^0 \bar{K}^0}$ are the three-vector momentum of the charged and neutral kaons, respectively. Note that there exists a sign between $g_{\rho K^+ K^-}$ and $g_{\rho K^0 \bar{K}^0}$ which brings cancellation between those two terms on the right-hand side of Eq. (18). At the mass of the ϕ meson, we obtain $\epsilon_{\phi\rho} = (9.51 - i3.31) \times 10^{-4}$ as an effective strong isospin-violating coupling for $\phi \rightarrow \rho^0$. This result can be compared with the intermediate meson transition in Eq. (2.10) of Ref. [21] apart from factor D_ρ , while the EM part has been contained in Eqs. (6) and (7).

The ω - ρ^0 strong mixing occurs only via intermediate charged pion loop transition as illustrated by Fig. 5(b). The transition amplitude is similar to that for ϕ - ρ^0 mixing, from which the strong isospin-violating coupling strength can also be defined,

$$\epsilon_{\omega\rho} \equiv \frac{1}{6\pi\sqrt{s}D_\rho} g_{\omega\pi^+\pi^-} g_{\rho\pi^+\pi^-} P_{\pi^+\pi^-}^3(s). \quad (19)$$

At the mass of ϕ meson, we obtain $\epsilon_{\omega\rho} = (13.7 - i4.8) \times 10^{-3}$, which is larger than that $\epsilon_{\phi\rho}$. However, we note in advance that the ω - ρ^0 mixing effects are negligibly small at the ϕ mass.

With all the contributing amplitudes above combined, the total transition amplitude can be expressed as

$$M_{fi} = M_{fi}^{I=1} + M_{fi}^{I=0}, \quad (20)$$

with

$$M_{fi}^{I=0} = M_{fi}^{EM-I=0} + e^{i\delta_L} (M_{fi}^{Loop-I=0} + M_{fi}^{mixing-I=0}), \quad (21)$$

where δ_L is the phase angle for the EM and loop transition amplitudes, and will be determined by the experimental data. The relative phase between $M_{fi}^{Loop-I=0}$ and $M_{fi}^{mixing-I=0}$ is given by the effective Lagrangian.

The differential cross section can thus be obtained:

$$\frac{d\sigma}{d\Omega} = \frac{1}{64\pi^2 s} \frac{|\mathbf{p}_f|}{|\mathbf{p}_e|} \frac{1}{4} \sum_{spin} |M_{fi}|^2 \quad (22)$$

where \mathbf{p}_e is the magnitude of the three-vector momentum of the initial electron (positron) in the overall c.m. system. We can neglect the mass of the electron, and have $|\mathbf{p}_e| = E_{cm}/2$.

In experiment, by defining the background cross section $\sigma_0(\sqrt{s})$ (from $I = 1$ transitions and $I = 0$ ω excitation), the full cross section can be parameterized as [26, 27, 28]:

$$\sigma(\sqrt{s}) = \sigma_0(\sqrt{s}) \left| 1 - Z \frac{M_\phi \Gamma_\phi}{D_\phi} \right|^2, \quad (23)$$

where M_ϕ and Γ_ϕ are the ϕ mass and width and $D_\phi = M_\phi^2 - s - i\sqrt{s}\Gamma_\phi$ is the inverse propagator of the ϕ meson; Z is a complex interference parameter that equals to the ratio of ϕ excitation amplitude to the background terms and describes the energy evolution of their relative phase. In our model, apart from calculating the cross sections, we shall also extract this quantity in order to compare with the values fitted in experiment [1, 2].

III. NUMERICAL RESULTS

The $I = 1$ components from the low-lying states ρ and $\rho'(1450)$ play an important role of background to the ϕ meson excitations, while we find that the ω contribution to the background via ω - ρ^0 mixing is negligibly small in the vicinity of the ϕ mass. In the VMD model the ρ contribution is relatively better controlled with its well-determined total and partial widths [4]. In contrast, the experimental status for $\rho'(1450)$ is still not well-established. This unavoidably leads to large uncertainties with its contributions. Interestingly, it shows that the side-band cross sections are essential for determining the contributions from ρ' . Since the exclusive contributions from ρ meson with $M_\rho = 775.0$ MeV and $\Gamma_\rho(M_\rho^2) = 149.4$ MeV still significant underestimate the side-band cross sections, it is a signal indicating that additional $I = 1$ components are needed. Nevertheless, it determines a constructive relative phase between ρ and ρ' terms in Eq. (5), i.e. $\delta_1 = 180^\circ$, which is the same as [13, 28, 29].

By adopting the PDG values for the $\rho'(1450)$, i.e. $M_{\rho'} = 1.459$ GeV, $\Gamma_{\rho'}(M_{\rho'}^2) = 147$ MeV and $\mathcal{B}_{\rho' \rightarrow \omega\pi^0} = 21\%$ [4], we find that it is still far from sufficient to account for the cross sections away from the ϕ mass. In particular, it shows that the cross section is not sensitive to the ρ' mass, but quite sensitive to its total width, due to the requirement of a stronger coupling to $\omega\pi^0$. This suggests that higher ρ states are also needed. At the ϕ mass we find that the effects of including higher ρ states simply enhance the $I = 1$ cross sections and the behavior of the energy dependence is not sensitive to the presence of another ρ state, e.g. $\rho(1700)$. Since the total width for $\rho'(1450)$ still has large uncertainties, we simply leave it to be determined by the side-band cross sections to take into account the possible contributions from higher ρ state.

The above features allow us to numerically fit the model parameters with the new and high-precision data from KLOE. In Ref. [2] the ϕ excitation cross sections are measured in both $e^+e^- \rightarrow \omega\pi^0 \rightarrow$

$\pi^+\pi^-\pi^0\pi^0$ and $\gamma\pi^0\pi^0$. With ω dominantly decaying into $\pi^+\pi^-\pi^0$, much smaller experimental uncertainties are achieved in the 4π production channel than in $\gamma\pi^0\pi^0$. These accurate data provide a stringent constraint on our model parameters.

In total, we have three parameters to be determined by the experimental data, i.e. a phase angle δ_L in Eq. (20), the form factor parameter α , and the total width $\Gamma_{\rho'}$ for ρ' . Two fits are carried out as an investigation of the parameter space. In Fit-I, we fix the phase angle $\delta_L = -90^\circ$ while leave α and $\Gamma_{\rho'}$ to be determined by the data. In Fit-II, we free these three parameters to let them be fitted by the data.

In Table I, the fitted parameters are listed. It shows that with $\delta_L = -90^\circ$ fixed in Fit-I, the reduced χ^2 value is much larger than that in Fit-II. Comparing these two fits, we see that $\delta_L = -111.6^\circ \pm 2.3^\circ$ is favored by the data while the fitted values for the other two parameters are consistent.

We list the branching ratios extracted from these two fits in Table II, and compare them with the PDG [4] and KLOE results [1, 2]. The ϕ - ρ^0 strong mixing is relatively small and independent of those parameters. Therefore, it keeps the same for both fits and contributes an exclusive branching ratio of 0.37×10^{-5} . The EM amplitudes have dependence on the ρ' width, which leads to small differences between these two fits. We then notice that significant differences between these two fits arise from the meson loop contributions. In Fit-I, the loop contributions constructively interfere with other transitions and lead to a relatively larger branching ratio, $BR_{\phi \rightarrow \omega\pi^0} = 4.29 \times 10^{-5}$, while in Fit-II the loop transition amplitude has a destructive effect and gives $BR_{\phi \rightarrow \omega\pi^0} = 2.83 \times 10^{-5}$. This is a novel feature arising from the precise data [2].

To disentangle this interesting phenomenon, we plot cross sections from different transitions in Fig. 6 for these two fits. It shows that Fit-II accounts for the data perfectly while Fit-I exhibits some discrepancies. The following points can be learned:

i) The extracted branching ratio is very sensitive to the line shape of the ϕ meson dip. This can be recognized by comparing the previous KLOE data [1] and the new one [2]. In Ref. [1] the relatively large uncertainties allow us to fix $\delta_L = -90^\circ$ to produce a result similar to Fit-I, i.e. $BR_{\phi \rightarrow \omega\pi^0} = 4.29 \times 10^{-5}$. But with data from Ref. [2], Fit-I exhibit obvious deviations from the precise data. In contrast, the success of Fit-II with a varying δ_L suggests a stringent constraint from the data.

ii) The side-band cross sections are important for determining the background contributions. As shown by the solid curve for the full calculation, at the energies away from the ϕ mass, the contributions from the ϕ excitation die out quickly, and the cross sections are dominated by the $I = 1$ components.

iii) The extracted branching ratio from Fit-II is smaller than the result from Refs. [1, 2] and PDG [4]. In our calculation it is due to the constraint from the line shape which requires a destructive phase between the EM and loop transition amplitudes. We also find that the branching ratio extraction is very sensitive to the background cross sections. It should be noted that although we can directly calculate the cross section for $e^+e^- \rightarrow \omega\pi^0 \rightarrow 4\pi$, the experimental extraction of this quantity needs understanding of non- $\omega\pi^0$ background which contribute to the 4π final state [2].

iv) Our calculations show that the ω - ρ^0 mixing effects are negligibly small at the ϕ mass region as illustrated by the dot-dot-dashed curved in the lower panels of Fig. 6.

In order to learn more about the underlying dynamics and clarify the interferences among different transitions, we make a further analysis of the amplitudes. In Fig. 7, we present the real and imaginary part of the exclusive transitions apart from the common factor $\bar{v}^{(s')}(p'_e)(-ie\gamma^\nu)u^s(p_e)\varepsilon_{\alpha\beta\mu\nu}p_\omega^\alpha\varepsilon_\omega^\beta p_\pi^\mu$. The solid lines denote the real and imaginary part of the background amplitude while the others are ϕ excitation amplitudes from EM, t -channel loop transitions, and s -channel ϕ - ρ^0 mixing. Their relative phases respect to the background terms are included. The visible difference between Fit-I (left panel) and Fit-II (right panel) is rather small though it can be seen that the t -channel loop amplitude plays a role to change the line shape due to the change of phase angle δ_L .

By extracting the Z parameter defined in Eq. (23), such a small difference can be highlighted due to the change of the background in these two fits. As shown by Fig. 8, both the real and imaginary part of Z turn out to be flat in terms of \sqrt{s} . The slight energy-dependence shows that the background contributions (dominated by $I = 1$ component) cannot come from a single isovector excitation. Their signs clearly indicate the destructive interferences between the ϕ excitation and the background terms.

At the ϕ mass, we extract the real and imaginary part of Z and compare them with the experimental results from KLOE [1, 2] etc. As shown by Tab. III, the extracted real and imaginary part of Z at the ϕ mass are basically in agreement with the data [1, 26, 27, 28] except that $\text{Re}Z$ from Fit-II appears

to be relatively small. This is again due to the difference of the background terms denoted by the extracted values for $\sigma_0^{4\pi}(M_\phi)$. It can be shown that with $\sigma_0^{4\pi}(M_\phi) = 7.12$ nb, $\text{Re}Z = 0.065 \pm 0.002$, and $\text{Im}Z = -0.103 \pm 0.005$, the cross section for $e^+e^- \rightarrow \omega\pi^0 \rightarrow 4\pi$ at $\sqrt{s} = M_\phi$ can be reproduced. Comparing our Fit-II results with Ref. [2], the sensitivity of the ϕ branching ratio to the background terms can be recognized. Note that the values for $\sigma_0^{4\pi}(M_\phi)$ in Tab. III from Refs. [1, 2] include about 12% contaminations from resonance background.

In Fig. 9, we plot the branching ratio dependence on the form factor parameter α with δ_L and $\Gamma_{\rho'}$ fixed as in Fit-I and II. It shows that over a broad range of α , the branching ratio does not vary drastically. The uncertainties of the fitted values for α in Fit-I and II are about 5% (see Tab. I), which suggest a well constraint of this parameter. It is also an indication that the loop integrals are well tamed.

IV. SUMMARY

The precise measurement of the ϕ excitation in $e^+e^- \rightarrow \omega\pi^0$ [2] as a consequence of interferences between the $I = 1$ and $I = 0$ components in the transition amplitudes provides an opportunity to study the isospin violation mechanisms at low energies. We investigate this process by quantifying the isospin violations in both EM and strong transitions. The $I = 1$ and $I = 0$ EM contributions are studied in the VMD model, while the $I = 0$ strong isospin violating process is described by the t -channel OZI-rule-evading intermediate-mesons-exchange loops and s -channel ϕ - ρ^0 mixing. This is an improved effective Lagrangian approach compared with our early study in Ref. [3] where the s -channel ϕ - ρ^0 mixing was overlooked.

In $e^+e^- \rightarrow \omega\pi^0$, the side-band cross sections provide a strong constraint on the $I = 1$ EM transitions. Contributions from ω meson excitation is also included though it turns out to be negligibly small. In the calculation we find that the cross section of $e^+e^- \rightarrow \omega\pi^0$ has evident width-dependence on the ρ' which contributes to the $I = 1$ transition amplitudes. In the previous work for $\phi \rightarrow \omega\pi^0$ [3], we did not include the ρ' due to lack of constraint on it. By fitting the new KLOE data [2], we succeed in constraining the model parameters, i.e. phase angle δ_L , form factor parameter α , and the total width $\Gamma_{\rho'}$ of ρ' . We show that there exists a strong correlation between the OZI-rule-evading and strong isospin violation mechanisms. We also find that the extracted branching ratio for $\phi \rightarrow \omega\pi^0$ is very sensitive to the line shape of the cross sections in the vicinity of ϕ excitation and the background estimate. Our result turns to be smaller than that given by Ref. [2].

It is worth noting that a relatively broad ρ' state is strongly favored by the newly published KLOE data [1]. Although it is not possible to answer whether an additional broad ρ' in addition to the $\rho'(1450)$ is needed, our results shed some light on this puzzling question in its interference with isospin violating transitions. It is also worth mentioning that there exist some hints of broad ρ' states around 1.2~ 1.6 GeV from experiments [30, 31]. Further theoretical investigation on $e^+e^- \rightarrow \omega\pi^0$ over a broader energy region, and precise measurement of the cross sections may be able to clarify such questions.

Acknowledgement

Useful discussions with C. Hanhart, S. Narison, J.-M. Richard, and B.S. Zou are acknowledged. This work is supported, in part, by the National Natural Science Foundation of China (Grants No. 10675131 and 10491306), Chinese Academy of Sciences (KJCX3-SYW-N2), and the U.K. EPSRC (Grant No. GR/S99433/01).

-
- [1] F. Ambrosino *et al.* [KLOE collaboration], arXiv:0707.4130 [hep-ex].
 - [2] F. Ambrosino *et al.* [KLOE collaboration], Phys. Lett. B **669**, 223 (2008) [arXiv:0807.4909 [hep-ex]].
 - [3] G. Li, Q. Zhao and B. S. Zou, Phys. Rev. D **77**, 014010 (2008) [arXiv:0706.0384 [hep-ph]].
 - [4] W. M. Yao *et al.* [Particle Data Group], J. Phys. G **33**, 1 (2006).

- [5] G. A. Miller, B. M. K. Nefkens and I. Slaus, Phys. Rept. **194**, 1 (1990).
 [6] A. Bramon, Phys. Rev. D **24**, 1994 (1981).
 [7] J.F. Donoghue, B.R. Holstein, and D. Wyler, Phys. Rev. Lett. **69**, 3444 (1992).
 [8] L. Ametller, C. Ayala and A. Bramon, Phys. Rev. D **30**, 674 (1984).
 [9] S.A. Coon, B.H.J. McKellar, and M.D. Scadron, Phys. Rev. D **34**, 2784 (1986).
 [10] S. A. Coon and R. C. Barrett, Phys. Rev. C **36** (1987) 2189.
 [11] H. Genz and S. Tatur, Phys. Rev. D **50**, 3263 (1994).
 [12] T. Bauer and D. R. Yennie, Phys. Lett. B **60**, 169 (1976).
 [13] R. R. Akhmetshin *et al.* [CMD-2 Collaboration], Phys. Lett. B **562**, 173 (2003) [arXiv:hep-ex/0304009].
 [14] V. L. Eletsky, B. L. Ioffe and Y. I. Kogan, Phys. Lett. B **122**, 423 (1983).
 [15] S. Narison and N. Paver, Z. Phys. C **22**, 69 (1984).
 [16] M. Lublinsky, Phys. Rev. D **55**, 249 (1997) [arXiv:hep-ph/9608331].
 [17] G. Li, Q. Zhao and C. H. Chang, J. Phys. G: Nucl. Part. Phys. **35**, 055002 (2008). arXiv:hep-ph/0701020.
 [18] A. Aloisio *et al.* [KLOE Collaboration], Phys. Lett. B **561**, 55 (2003); **609**, 449(E) (2005); arXiv:hep-ex/0303016.
 [19] H. J. Lipkin, Nucl. Phys. B **291**, 720 (1987).
 [20] H. J. Lipkin, Phys. Lett. B **179**, 278 (1986).
 [21] N.N. Achasov and A.A. Kozhevnikov, Int. J. Mod. Phys. **A 7**, 4825 (1992).
 [22] N.A. Tornqvist, Annals Phys. **123**, 1 (1979).
 [23] M. P. Locher, Y. Lu and B. S. Zou, Z. Phys. A **347**, 281 (1994) [arXiv:nucl-th/9311021].
 [24] X. Q. Li, D. V. Bugg and B. S. Zou, Phys. Rev. D **55**, 1421 (1997).
 [25] X. Q. Li and B. S. Zou, Phys. Lett. B **399**, 297 (1997) [arXiv:hep-ph/9611223].
 [26] M. N. Achasov *et al.*, Nucl. Phys. B **569**, 158 (2000) [arXiv:hep-ex/9907026].
 [27] M. N. Achasov *et al.*, Phys. Lett. B **449**, 122 (1999) [arXiv:hep-ex/9901020].
 [28] V. M. Aulchenko *et al.*, Jou. Exp. Th. Phys. **90**, 927 (2000).
 [29] A. B. Clegg and A. Donnachie, Z. Phys. C **62**, 455 (1994).
 [30] C. Amsler *et al.* [Crystal Barrel Collaboration], Nucl. Phys. **A 740**, 130 (2004).
 [31] M. Ablikim *et al.* [BES Collaboration], Phys. Rev. Lett. **97**, 142002 (2006).

Parameter	θ	α	$\Gamma_{\rho'}$ (MeV)	$\chi^2/d.o.f$
Fit-I	-90.0° (fixed)	1.125 ± 0.052	674 ± 6	5.71
Fit-II	$-111.6^\circ \pm 2.3^\circ$	1.244 ± 0.051	683 ± 6	0.54

TABLE I: The parameters fitted in Fit-I and Fit-II schemes.

Branching ratio ($\times 10^{-5}$)	EM	Meson loop	ϕ - ρ^0 mixing	Total	PDG [4]	Exp [1]	Exp [2]
Fit-I	2.95	0.93	0.37	4.29	$5.2^{+1.3}_{-1.1}$	5.63 ± 0.70	4.4 ± 0.6
Fit-II	2.97	1.14	0.37	2.83			

TABLE II: Branching ratios for $\phi \rightarrow \omega\pi^0$ extracted from our model with two different fitting schemes. Experimental data [1, 2, 4] and exclusive branching ratios from EM, t -channel meson loop transitions, and s -channel ϕ - ρ^0 mixing are also listed.

	$\sigma_0^{4\pi}(M_\phi), (nb)$	Re Z	Im Z
Ref. [26]	$7.32 \pm 0.14 \pm 0.38$	$0.110 \pm 0.019 \pm 0.003$	$-0.129 \pm 0.025 \pm 0.005$
Ref. [27]	$7.28 \pm 0.18 \pm 0.80$	$0.104 \pm 0.028 \pm 0.006$	$-0.118 \pm 0.030 \pm 0.009$
Ref. [28]	7.34 ± 0.14	0.112 ± 0.019	-0.129 ± 0.025
Ref. [1]	$(8.12 \pm 0.14)^\dagger$	0.097 ± 0.012	-0.133 ± 0.009
Ref. [2]	$(7.89 \pm 0.06 \pm 0.07)^\dagger$	$0.106 \pm 0.007 \pm 0.004$	$-0.103 \pm 0.004 \pm 0.003$
Fit-I	7.08 ± 0.04	0.107 ± 0.005	-0.110 ± 0.009
Fit-II	7.12 ± 0.03	0.065 ± 0.002	-0.103 ± 0.005

TABLE III: The interference parameter Z extracted from our model by two different fitting schemes at the ϕ mass is compared with experimental results. Note that the values of $\sigma_0^{4\pi}(M_\phi)$ labeled by “ \dagger ” contain about 12% non- $\omega\pi^0$ contaminations [1, 2].

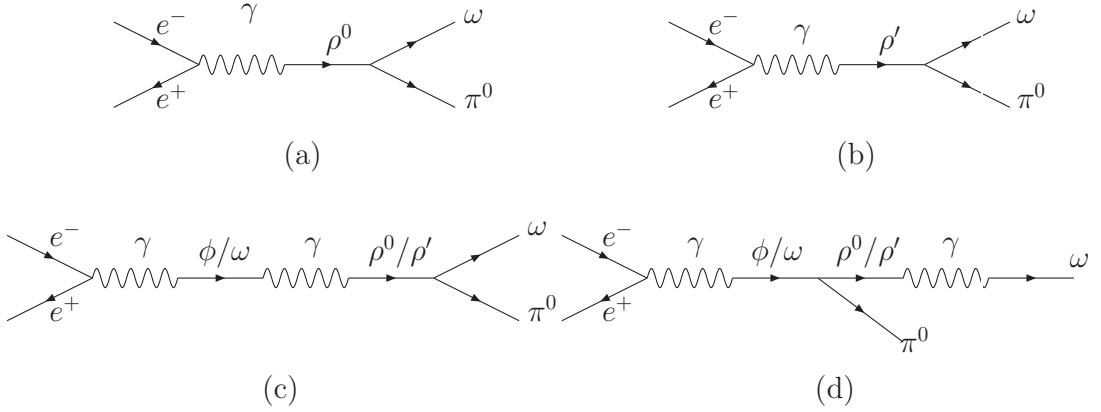


FIG. 1: The schematic diagrams for $I = 1$ [(a) and (b)] and $I = 0$ EM transitions [(c) and (d)].

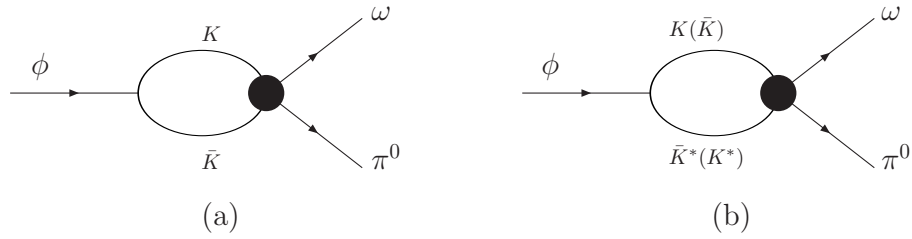


FIG. 2: The schematic diagrams for $\phi \rightarrow \omega\pi^0$ via the OZI-rule-evading intermediate meson loop transitions.

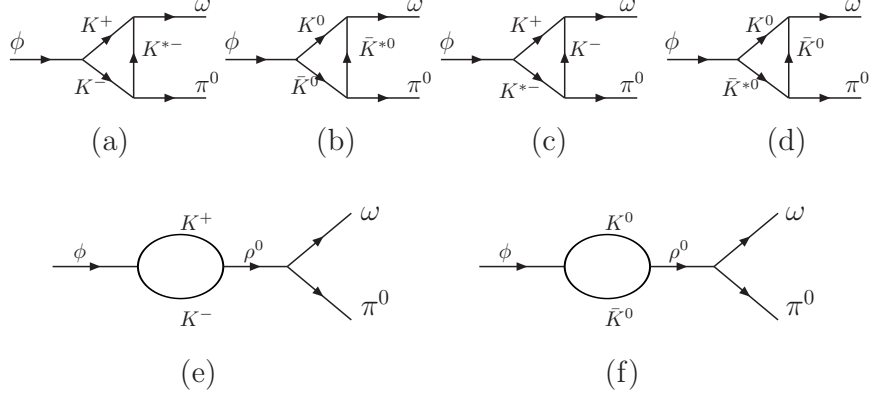


FIG. 3: The transition mechanisms for $\phi \rightarrow \omega\pi^0$ via t -channel [(a)-(d)] and s -channel transitions [(e) and (f)].

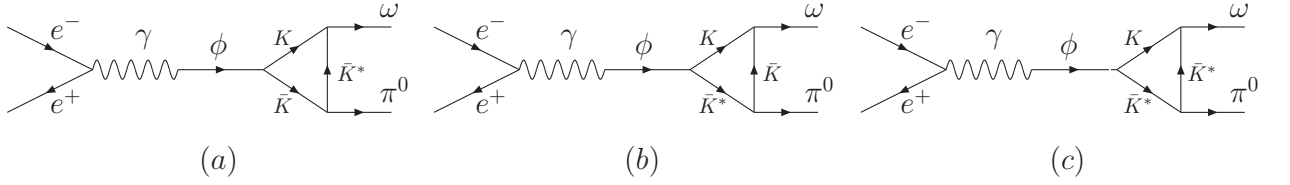


FIG. 4: The schematic diagrams of $I = 0$ transitions for $e^+e^- \rightarrow \omega\pi^0$ via $KK(K^*)$, $KK^*(K)$ and $KK^*(K^*)$ intermediate meson loops.

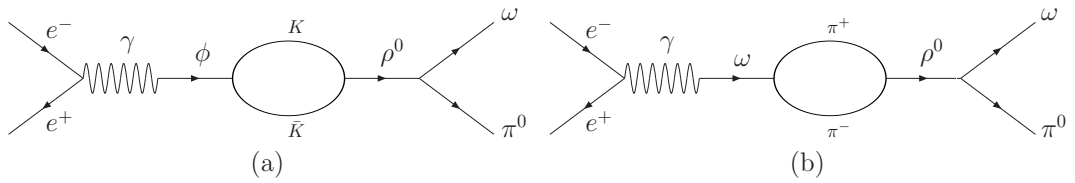


FIG. 5: The schematic diagrams of $I = 0$ transitions for $e^+e^- \rightarrow \omega\pi^0$ via ϕ - ρ^0 mixing.

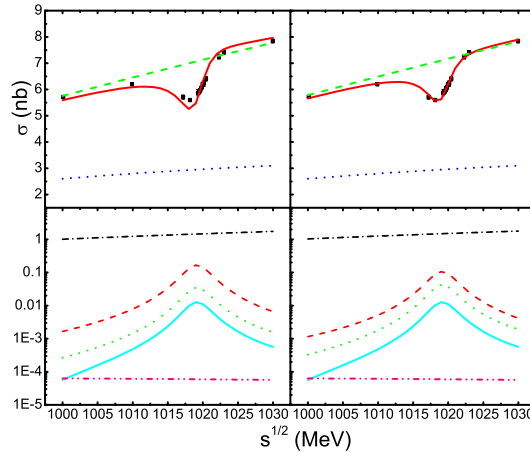


FIG. 6: (color online). The \sqrt{s} -dependence of the total cross section for $e^+e^- \rightarrow \omega\pi^0$ fitted in Fit-I (left) and Fit-II (right). The data are from KLOE measurement [2]. In the lower panels, the dotted curves denote the exclusive t -channel meson loop contributions, the solid lines denote the contributions from the ϕ - ρ^0 mixing, the dot-dot-dashed lines denote the contributions from the ω - ρ^0 mixing, while the dashed ones for the inclusive cross sections for ϕ excitations (EM plus strong isospin violation). The dot-dashed lines stand for cross sections from $\rho'(1450)$ with fitted total widths. In the upper panels, the dotted lines denote the contributions from the ρ meson, while the dashed lines are for the inclusive contributions from background including the dominated $I = 1$ component (ρ plus $\rho'(1450)$) and a small $I = 0$ ω excitation. The solid curves are the full model results.

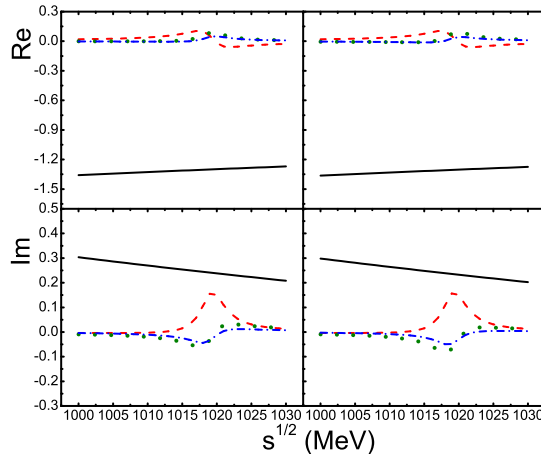


FIG. 7: (color online). Energy evolution of the real (upper panel) and imaginary (lower panel) amplitudes given by Fit-I (left) and Fit-II (right). The solid lines denote the amplitude for the background terms (dominated by $I = 1$ component); the dashed lines stand for $I = 0$ EM transition amplitude, the dotted lines denote the $I = 0$ t -channel transitions, while the dash-dot lines for the s -channel ϕ - ρ^0 mixing. A common factor $\bar{v}^{(s')}(p'_e)(-ie\gamma^\nu)u^s(p_e)\varepsilon_{\alpha\beta\mu\nu}p_\omega^\alpha\varepsilon_\omega^\beta p_\pi^\mu$ in the transition amplitudes has been removed.

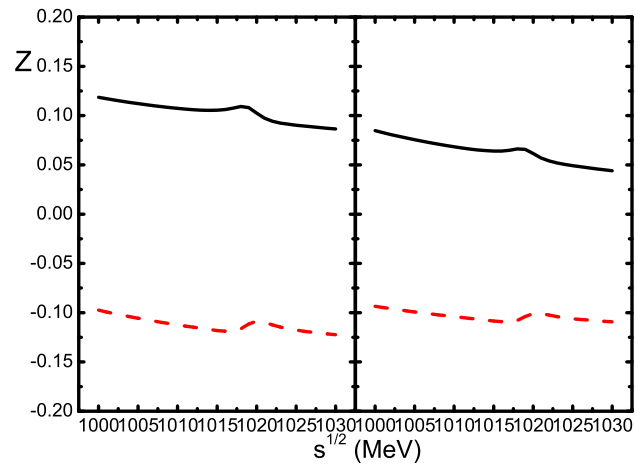


FIG. 8: (color online). Energy evolution of parameter Z extracted from Fit-I (left) and Fit-II (right). The solid lines stand for the real part while the dashed lines for the imaginary part.

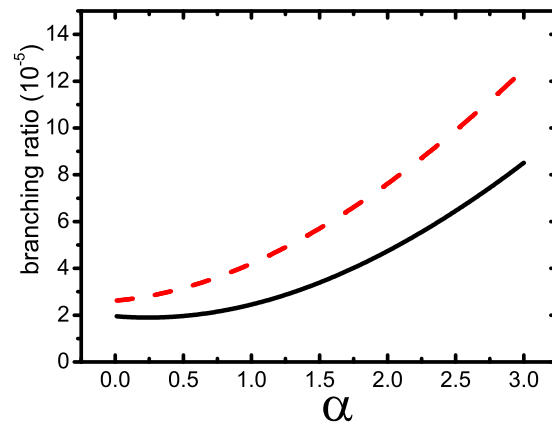


FIG. 9: The α -dependence of the $\phi \rightarrow \omega\pi^0$ branching ratio in Fit-I (dashed) and Fit-II (solid).